Modulating Calcitonin Fibrillogenesis

AN ANTIPARALLEL α-HELICAL DIMER INHIBITS FIBRILLATION OF SALMON CALCITONIN*

Giuseppina Andreotti and Andrea Motta‡

From the Istituto di Chimica Biomolecolare del Consiglio Nazionale delle Ricerche (CNR), Comprensorio Olivetti, Edificio 70, Via Campi Flegrei 34, I-80078 Pozzuoli (Napoli), Italy

We have investigated the prefibrillar state of salmon (s) and human (h) calcitonin (CT). Size exclusion chromatography at pH 3.3 and 7.4 indicates that sCT is present in solution as a dimer, whereas hCT elutes as a monomer at pH 3.3 and as monomer-dimer at pH 7.4. Guanidine hydrochloride unfolding experiments show that dimerization is stabilized by hydrophobic interactions. We investigated the dimeric structure by multidimensional nuclear magnetic resonance spectroscopy and calculations by using an sCT mutant (LAsCT) in which Pro[23] and Arg[24] were substituted for Leu[23] and Ala[24]. As indicated by the Leu[9]–Tyr[27] and Leu[12]–Leu[19] contacts, the mutated hormone forms a head-to-tail dimer whose basic unit is an α-helix in the region Leu[12]–Tyr[22]. The solution behavior of LAsCT is identical to that of sCT, so the dimeric structure can safely be extended to sCT: we believe that such a structure inhibits fibril maturation in sCT. No stable dimer was observed for hCT, which we attributed to the absence of a defined helical structure. However, we suggest that intermolecular collisions of short ordered regions (for example, a sequence of turns) in hCT favors intermolecular contacts, and specific orientation can be obtained through hydrogen bond formation involving Tyr[12], Phe[16], and Phe[19], with the aromatic ring acting as an acceptor. Taken together, our results indicate that hCT fibrillation can be reduced by favoring a helical dimer, obtainable by replacing the three aromatic amino acids with leucines.

Protein amyloid fibrils are found in about 20 diseases of unrelated origin, including Alzheimer's disease, diabetes mellitus (type II diabetes), familial amyloidosis, light chain amyloidosis, transmissible spongiform encephalopathies, and Parkinson's disease (1). It is not known which structural features cause specific proteins to form amyloid fibrils *in vivo*; however, evidence is accumulating that aggregation is initiated from specific regions within a polypeptide chain (2–6).

Human calcitonin (hCT),[1] a 32-amino-acid polypeptide hormone of ~3.4 kDa (Scheme 1) produced by thyroidal C-cells, forms amyloid fibrils associated with medullary carcinoma of the thyroid (7). Synthetic hCT also forms amyloid fibrils *in vitro*, with a morphology similar to the thyroid deposits (8). Calcitonin (CT) can be used to treat various diseases including Paget's disease and osteoporosis (9), but the tendency of hCT to associate into amyloid fibrils at physiological pH limits its efficacy as a drug. Salmon CT (sCT) (Scheme 1), the clinically used alternative to hCT, causes immunogenic reactions (10). Therefore, understanding the mechanism of amyloid formation by hCT and controlling this process are important not only in the context of amyloid formation but also as a step toward improved therapeutic use of CT.

The detailed molecular mechanism of CT fibril formation is not yet well understood. It has been proposed that the first step is a homogeneous association of α-helices to form the nucleus of a fibril followed by an autocatalytic heterogeneous fibrillation of β-sheets to form a mature fibril (11).

It has been suggested that hydrophobic interactions favor the formation of α-helical bundles, whereas charged amino acids regulate the β-sheet association (12). The fibrillation of sCT is much slower than hCT, requiring more than 8 months as compared with 21 min for hCT at 1 mg/ml and pH 7.4 (8); furthermore, the fibrillation of hCT at low pH is slower than that at physiological pH (8). Considering that the proposed fibrillation mechanism involves a homogeneous aggregation of α-helices, it is surprising that sCT does not fibrillate, despite having a helical propensity higher than hCT (13, 14).

To understand the structural determinants that cause the differing fibrillation mechanism of hCT and sCT, we investigated the prefibrillar state of both hormones. Size exclusion chromatography at pH 3.3 and 7.4 indicate that sCT is present in solution as a dimer. hCT is eluted as a monomer at pH 3.3 but is in equilibrium between dimer and monomer at pH 7.4. The structure of dimeric sCT was investigated by NMR spectroscopy and calculations by resorting to an sCT mutant (referred to as LAsCT) in which Pro[23] and Arg[24] were substituted for Leu[23] and Ala[24] (Scheme 1). LAsCT showed properties identical to those of sCT, the only difference being the stability and the length of the amphipathic α-helix in membrane-like environment.[2] We report here that, in water, LAsCT forms an α-helical head-to-tail dimer in the region Leu[12]–Tyr[22]. Guanidine HCl unfolding experiments at physiological pH indicate that hydrophobic interactions are responsible for the association of all three calcitonins. The striking similarity between LAsCT and sCT strongly suggests that sCT dimerizes via the hydrophobic face of the helix using the leucines at sites 12, 16, and 19. On the contrary, hCT, in which the key leucines are

---

‡ To whom correspondence should be addressed. Tel. 39-081-8675-228; Fax: 39-081-8041-770; E-mail: amotta@icmib.na.cnr.it; andrea.motta@icb.cnr.it.

[1] The abbreviations used are: CT, calcitonin; hCT, human CT; sCT, salmon CT; LAsCT, sCT with Pro[23]–Arg[24] substituted by Leu-Ala; BPTI, bovine pancreatic trypsin inhibitor; MD, molecular dynamics; NOE, nuclear Overhauser enhancement; NOESY, nuclear Overhauser spectroscopy; r.m.s., root mean square; TOCSY, total correlation spectroscopy.

[2] G. Andreotti, B. López Méndez, P. Amodeo, M. A. Castiglione Morelli, H. Nakamuta, and A. Motta, submitted.

```
        1          10              20              30
hCT   C G N L S T C M L G T Y T Q D F N K F H T F P Q T A I G V G A P

sCT     C S N L S T C V L G K L S Q E L H K L Q T Y P R T N T G S G T P

LAsCT   C S N L S T C V L G K L S Q E L H K L Q T Y L A T N T G S G T P
```

SCHEME 1. **Amino acid sequences of hCT, sCT, and LAsCT.** In the 12–22 region, aromatic residues are in *bold*, and leucines are *shaded*. Mutations of Pro23–Arg24 in sCT to Leu23–Ala24 in LAsCT are in *underlined italics*.

substituted by aromatic residues (Scheme 1), takes up a sequence of turns in the central region.

An important issue is whether aromatic amino acids in hCT have a driving role in fibril formation (5). Our results support this idea. The absence of a defined helix in the central region of hCT corroborates the requirement for fibrillation of specific chemical properties in a definite region of the hormone (5). Intermolecular collision of short ordered regions is a possible mechanism to bring together two molecules to allow chemical interaction. In particular, the presence of aromatic residues at sites 12, 16, and 19 in hCT would drive a specific orientation through hydrogen bond formation, the benzene ring acting as hydrogen bond acceptor. Such a mechanism could well explain fibril formation by short hCT-based peptides. Furthermore, leucines (but not aromatic residues) in the central region of sCT and LAsCT favor a stable prefibrillar helical dimer that prevents amyloid formation. We therefore propose that hCT fibrillation can be prevented by stabilizing a leucine-based helical dimer, which can be achieved by substituting aromatic amino acids for leucine residues at sites 12, 16, and 19. Biological support for our conclusion is given by a report showing a 20-fold increase of hCT hypocalcaemic potency, obtained by replacing aromatic amino acids by Leu residues (15). Finally, our finding strongly supports the hypothesis (16) that stabilization of an α-helix/β-strand-discordant stretch (*i.e.* an α-helix in a polypeptide segment that should form a β-strand according to secondary structure predictions) into α-helix avoids amyloid fibril formation.

EXPERIMENTAL PROCEDURES

Peptide Synthesis—sCT, LAsCT, and hCT (a gift from Dr. Nagana A. Goud, Bachem, Torrance, CA) were prepared by standard methods.

Size Exclusion Chromatography—Size exclusion chromatography was carried out at room temperature, using a 1.5 × 50-cm Sephadex G-50 Fine column at a flow rate of 0.3 ml/min. Chromatography was performed at pH 7.4, using 20 mM phosphate containing 100 mM NaCl, and at pH 3.3, using 20 mM acetate containing 100 mM NaCl. The concentrations used for hCT were as follows: 0.15, 0.36, and 1.33 mM at pH 3.3 and 0.081 and 0.31 mM at pH 7.4. The concentrations used for sCT and LAsCT were as follows: 0.40 and 0.45 mM at pH 3.3, and 0.58 mM at pH 7.4. Insulin B-chain (3.5 kDa) and bovine pancreatic tripsin inhibitor (BPTI, 6.6 kDa), both purchased from Sigma, were used as molecular weight standards. Peptide concentrations were determined by ultraviolet absorption spectroscopy using coefficients at 275 nm of 1531 and 1515 cm^{-1} M^{-1} for hCT, sCT, and LAsCT, respectively (17).

Circular Dichroism Spectroscopy—Measurements were performed on a Jasco-J710 spectropolarimeter connected to a water bath used to control the temperature of the cell. LAsCT CD spectra were recorded in the far UV region (200–240 nm) at 295 K and pH 3.3 (20 mM acetate, 100 mM NaCl) and 7.4 (20 mM phosphate, 100 mM NaCl) with a peptide concentration of 0.072 mM in a 1.0-cm path length cell. Spectra in the presence of 0.4 M SDS, at both pHs, were acquired with a peptide concentration of 0.41 mM in a 0.1-cm path length cell. A spectral bandwidth of 2.0 nm and a scan speed of 10 nm/min were used. The precision of the data was improved by averaging five scans, and the results are reported as mean residue ellipticity (θ). Prediction of percentages of secondary structure from CD spectra was obtained using the k2d software, a Kohonen neural network with a two-dimensional output layer (18, 19) (www.embl-heidelberg.de/~andrade/k2d).

Possible fibril formation of each peptide was monitored at 293 K with time course experiments for 24 h by following the ellipticity at 205 nm. Freshly dissolved peptide was used at different concentrations (0.030, 0.060, and 0.18 mM at pH 3.3 and 7.4, in 20 mM acetate and phosphate buffers, respectively, both containing 100 mM NaCl. CD spectra of

LAsCT and sCT samples corresponding to the above concentrations, as obtained from a sample of 0.59 mM kept at room temperature, were examined after 8 months.

Guanidine Denaturation—The guanidine hydrochloride denaturation studies of hCT, sCT, and LAsCT were carried out at 295 K in 100 mM phosphate buffer at pH 7.4. Mixtures of freshly prepared stock solutions of peptide, phosphate buffer, and guanidine hydrochloride were made to obtain denaturant concentration ranging from 0 to 4 M. The final peptide concentration was 0.1 mg/ml. Preliminary experiments showed that incubation of 30 min was sufficient to reach the equilibrium. Guanidine-induced unfolding was monitored by measuring ellipticity at 220 nm as a function of denaturant concentration. The CD spectrum of each sample was recorded between 210 and 230 nm in a 0.1-cm path length cell. A spectral bandwidth of 1.0 nm and a scan speed of 50 nm/min were used, and each spectrum was accumulated five times. All the spectra were corrected for the contribution of the buffer. The results are reported as mean residue ellipticity.

NMR Data Collection—All CT samples were prepared by dissolving the appropriate amounts of the peptide in 0.5 ml of ^{1}H$_2$O, ^{2}H$_2$O (90/10 v/v) to yield concentrations of 0.59 mM. Deuterated water was obtained from CortecNet (Paris, France).

^{1}H NMR spectra, recorded at 293 K and pH 3.3 and 7.4, were acquired on a Bruker DRX-500 spectrometer operating at 500 MHz using an inverse multinuclear probehead fitted with gradients along the *x*, *y*, and *z* axes. Spectra were referenced to sodium 3-(trimethylsilyl)-(2,2,3,3-^{2}H$_4$)propionate. Homonuclear two-dimensional clean TOCSY (20) and NOESY (21) spectra were recorded by incorporating the excitation sculpting sequence (22) for water suppression. We used a pulsed-field gradient double echo with a soft square pulse of 4 ms at the water resonance frequency, with the gradient pulses of 1 ms each in duration. 512 equally spaced evolution time period t_1 values were acquired, averaging 16 transients of 2048 points, with 6024 Hz of spectral width. Time domain data matrices were all zero-filled to 4096 in both dimensions, yielding a digital resolution of 2.94 Hz/point. Prior to Fourier transformation, resolution enhancement was applied with a Lorentz-Gauss window to both t_1 and t_2 dimensions for all the experiments. NOESY spectra were obtained with different mixing times (100, 200, 300, and 400 ms), TOCSY experiments were recorded with a spin-lock period of 64 and 96 ms, achieved with the MLEV-17 pulse sequence

Structure Calculations—Distance restraints for structure calculations were obtained by integrating the volumes of NOE peaks at different mixing times and representing the buildup of the NOEs by a second-order polynomial. The corresponding interproton distances were calculated using an r^{-6} dependence of the initial slope. An upper bound was set for all distance restraints to 10% above the calculated distance, whereas the lower bound was set conservatively to 0.25 nm, representing a value close to van der Waals contact. For the methyl protons, a correction of 0.03 nm was made (23). φ and ψ dihedral angle restraints were derived from $^3J_{NH\alpha}$ coupling constants. The structure of the monomer was calculated with 230 NOEs (109 intraresidue, 85 sequential (αCH$_i$–NH$_{i+1}$, βCH$_i$–NH$_{i+1}$, and NH$_i$–NH$_{i+1}$), and 36 medium range (αCH$_i$–NH$_{i+n}$, $n \geq 2$, and αCH$_i$–βCH$_{i+3}$)). For the dimer, we used a total of 464 NOEs, which include four intermolecular NOEs defining the mutual orientation of single chains.

Model building and preliminary calculations were performed with the united atom model (24) with the SYBYL 6.2 package (Tripos Inc., St. Louis, MO). The solvation effects were approximated by using a distance-dependent dielectric constant $\epsilon = r$. A cutoff radius of 0.8 nm for non-bonded interactions, with a residue-based pair list generation routine, was used for all calculations. In the united atom model, distance restraints were included as C–C or C–N distance, increasing the upper limits calculated for interproton distances by 0.1 nm. Semiparabolic penalty functions were used with force constants in energy minimization and room temperature molecular dynamics (MD) of 83.33 kJ mol^{-1} radians^{-2} for dihedral restraints and 8.33 kJ mol^{-1} nm^{-2} for distance restraints. In simulated annealing and preliminary MD simulations, a time step of 1 fs was used, with no restraints on bond length. Simulated annealing runs were performed with different lengths (from 10 to 250 ps), temperatures (maximum values from 500 to 800 K, applied for 25–75% of the total time, cooling rates from 1 to 5 K ps^{-1}), and restraint force constant time profiles. Energy minimization and MD simulations with solvent were performed with the SANDER module of the AMBER 4.1 package. A time step of 2 fs, with rigid restraint of all bond lengths (SHAKE algorithm) (25, 26), and periodic boundary conditions were applied. All MD simulations were performed in the isothermal-isobaric ensemble (300 K, 1 atm), with a solvent box that initially extended 0.8 nm from the most external solute atom on each side of the box. Molec-
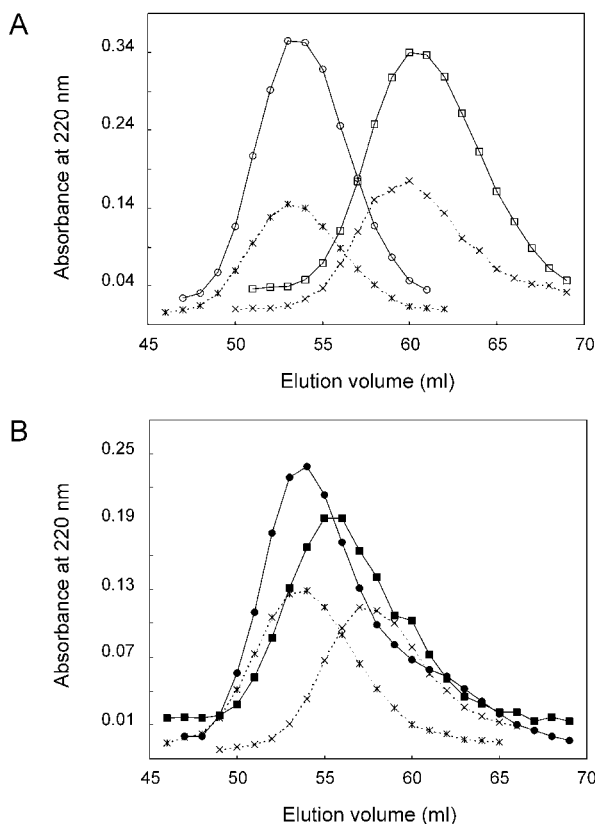
A

B

FIG. 1. **Molecular sizes by gel filtration of hCT and sCT (Sephadex G-50 column).** *A*, elution profiles for hCT ($\square$, 0.56 mg/ml) and sCT ($\bigcirc$, 0.60 mg/ml) in 20 mM acetate, 100 mM NaCl, pH 3.3. *B*, elution profiles for hCT ($\blacksquare$, 0.47 mg/ml) and sCT ($\bullet$, 0.88 mg/ml) in 20 mM phosphate, 100 mM NaCl, pH 7.4. Insulin B-chain ($\times$, 3.5 kDa) and BPTI (*, 6.6 kDa), used as molecular size standards, are also noted.

FIG. 2. **Guanidine hydrochloride denaturation profiles of hCT and sCT.** The mean residue ellipticity at 220 nm of hCT ($\blacksquare$) and sCT ($\bullet$), recorded at a concentration of 0.1 mg/ml, 100 mM phosphate, pH 7.4, and 295 K, is shown as a function of the denaturant concentration.

ular structures were drawn and analyzed with the graphics program MOLMOL (27).

RESULTS

Size Exclusion Chromatography—The apparent molecular weights of hCT and sCT at non-fibrillating concentration were measured by gel filtration on a Sephadex G-50 column using as eluents 20 mM phosphate containing 100 mM NaCl (pH 7.4) and 20 mM acetate containing 100 mM NaCl (pH 3.3). sCT (Fig. 1*A*, *open circles*) eluted at pH 3.3 with an apparent molecular mass of 6.6 kDa (compare with BPTI, 6.6 kDa, *stars*) instead of 3.4 kDa as indicated by its amino acid composition. On the contrary, hCT (*open squares*) eluted with an apparent molecular mass corresponding to that of the insulin B-chain (3.5 kDa, *crosses*). Therefore, whereas sCT elutes as a dimer, hCT appears as a monomer. Both elution patterns are symmetric, as are those of the two standards, and this implies the presence of a single species in solution.

At pH 7.4 (Fig. 1*B*), sCT shows an elution profile (*filled circles*) with a predominant component corresponding to the molecular weight of a dimer, with a slight tail due to the presence of a second minor component corresponding to sCT monomer. Such an asymmetry of the eluted peak is characteristic of a dissociating system (28), suggesting an equilibrium between the two forms strongly favoring the dimer. The elution pattern of hCT (Fig. 1*B*, *filled squares*) is asymmetric with a sharper front edge between monomer and dimer and a tail region showing a distinct second component corresponding to hCT monomer, suggestive of a slow equilibrium between the two forms.

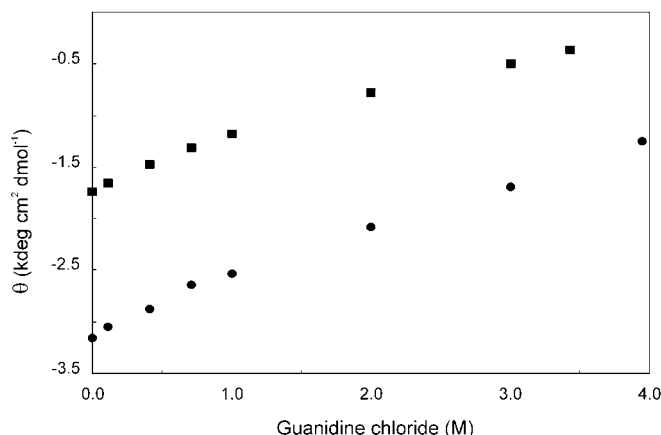*Denaturation with Guanidine Hydrochloride*—Fig. 2 depicts

the denaturation curves at pH 7.4 and 295 K, obtained by monitoring the hCT (*filled squares*) and sCT (*filled circles*) ellipticities at 220 nm as a function of guanidine HCl concentration. Upon addition of guanidine, we observed a reduction of ellipticity for both hormones. This is consistent with the presence of hydrophobicity-induced association for both hCT and sCT. Identical behavior was observed for sCT at pH 3.3 (not shown), supporting the relevance of hydrophobic association in the formation of the dimer at both acidic and physiological pH.

LAsCT, an sCT Mutant Used to Characterize the Dimer—The possibility of characterizing the sCT dimer relies on its stability in solution. In water, at physiological conditions, CD spectra indicate that neither hCT nor sCT have significant ordered structure (29). The reported α-helix percentages are ~8% for hCT and ~14% for sCT, with ~18% of turns. NMR NOESY experiments of hCT and sCT in water at pH 7.4 (not shown) indicated the presence of strong αCH_i–NH_{i+1} connectivities along the whole chain of hCT and sCT, and weak NH_i–NH_{i+1} connectivities concentrated in the 12–20 region and in the Cys^1–Cys^7 loop. Furthermore, we noticed the presence of scattered αCH_i–NH_{i+2} and βCH_i–NH_{i+1} connectivities. This finding argues for the presence of a structure fluctuating between an extended chain and a sequence of turns located in the central region of CT (30).

We synthesized the LAsCT mutant to lengthen and stabilize the helix. A detailed structural study by NMR spectroscopy and calculations of LAsCT in the presence of SDS[2] indicated that LAsCT does have a longer (Leu^4–Gly^{28}) and more stable helix than does sCT (Thr^6–Tyr^{22}). What structure does it assume in water? Fig. 3 shows the CD spectra of LAsCT at pH 7.4 and 295 K in water (*broken line*) and in SDS (*continuous line*). Estimation of the secondary structure by the k2d neural network algorithm (18, 19) suggests the presence of ~20% α-helix in water. In SDS, a dominant α-helix is clearly discernable, as two minima with high ellipticity values are observed at 220 and 208 nm. We estimated the presence of 56% α-helix, significantly lower than the 75% obtained by NMR studies. Therefore, although secondary structure estimation from CD spectra is less reliable than from NMR, we think that the detected helical percentage (~20%) indicates a sufficient stability to promote the dimer.

Possible fibril formation by LAsCT was examined (with time course) at pH 3.3 and 7.4 for freshly dissolved peptide at different concentrations (0.031, 0.060, and 0.18 mM). The ellipticity at 205 nm was monitored for 24 h without any appreciable variation of the signal. We also compared the CD spectra of the
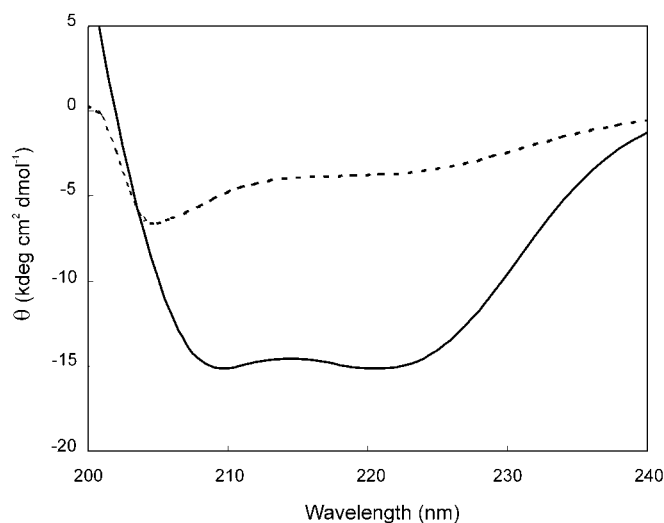
FIG. 3. **CD spectra of LAsCT.** Spectra were recorded at 295 K in 20 mM phosphate, 100 mM NaCl, pH 7.4, at a peptide concentration of 0.1 mg/ml (*dashed line*) and in 0.4 M SDS at a peptide concentration of 0.6 mg/ml (*continuous line*). The results are reported as mean residue ellipticity.

samples above with corresponding concentrations derived from a sample of 0.59 mM kept at room temperature for 8 months without showing macroscopic evidence of aggregation. The spectra from the two sets are identical, so we concluded that the fibrillation time for LAsCT is a slow process, similar to that reported for sCT (8).

Gel filtration experiments indicated that at pH 3.3 and 7.4, the elution patterns of LAsCT are symmetric and correspond to an apparent dimeric molecular weight. Finally, the denaturation curve at pH 7.4 is very similar to that observed for sCT, confirming the hydrophobic nature of the interactions stabilizing the dimer. Therefore, we conclude that, except for the longer helical segment, the solution behavior of LAsCT is identical to that of sCT.

LAsCT Forms an Antiparallel α-Helix Dimer in Water—The NMR spectral assignment of LAsCT was carried out at pH 3.3 and pH 7.4 by the homonuclear ^{1}H NMR approach (30). Identification of the complete spin systems of all 32 residues was based on TOCSY and NOESY experiments. The peptide secondary structure was delineated from qualitative analysis of the sequential (αCH_i–NH_{i+1} and NH_i–NH_{i+1}) and medium range (αCH_i–NH_{i+n}, $1 < n < 4$, and αCH_i–βCH_{i+3}) NOEs. Fig. 4*A* summarizes the observed NOEs at pH 7.4 and at a concentration of 0.59 mM. The central region of the peptide shows intense NH_i-NH_{i+1} NOEs, whereas the αCH_i–NH_{i+1} connectivities are weaker, implying a generally helical structure (30). This was clearly identified by αCH_i-NH_{i+3}, αCH_i–NH_{i+4} and αCH_i–βCH_{i+3} appearing in the region Leu[12]–Tyr[22] (Fig. 4*A*); the lack of such connectivities at the N- and C-terminal regions suggests a less organized structure. The presence of a helix in the Leu[12]–Tyr[22] region is also supported by $^3J_{HN\alpha} < 6$ Hz (30). Although without doubt the helical nature in the 12–22 region is established via sequential and medium range NOEs, the differentiation between an α-helix and a 3$_{10}$-helix is, however, more difficult. Actually, the fact that αCH_i–NH_{i+2} connectivities, not observable in an α-helix, are generally detected along the chain and in particular, in the Leu[12]–Tyr[22] region, suggests that we have a 3$_{10}$-helix. On the other hand, the presence of αCH_i–NH_{i+4} connectivities (Leu[12]–Leu[16], Ser[13]–His[17], His[17]–Thr[21], and Lys[18]–Tyr[22]), not observable in a 3$_{10}$-helix, also demonstrates that this part of the peptide could take up an α-helix. The simultaneous presence of NOEs peculiar to α- and 3$_{10}$-helices can be interpreted as evidence of flexibility (31).

Calculations (see below), however, indicate a preference for the α-helix. The helical wheel diagram (Fig. 4*B*) indicates that Leu[12], Leu[16], and Leu[19], and Ser[13], His[17], and Thr[21] are positioned on opposite sides of the helix, indicating an amphipatic helix whose hydrophobic face is composed of leucine residues.

Three-dimensional structures of LAsCT were generated as described under "Experimental Procedures." From the initial 60 structures, 30 were selected for further refinement. They had no violations of the upper and lower bounds of the NMR distance restraints greater than 0.10 and 0.12 nm, respectively, and did not predict any unobserved NOEs. They were subjected to restrained energy minimization using the AMBER package (see "Experimental Procedures"). The energies of these refined structures were all in the narrow range from −3,225 to −3,775 kJ·mol^{-1}. Refinement produced a decrease of the overall energy, but the NOE restraint energies underwent a small increase upon minimization. The overall agreement among individual conformers can be seen by global root mean square (r.m.s.) deviation. The average r.m.s. deviation between the 12 best structure pairs is 0.074 ± 0.016 nm for the backbone atoms in the 9–22 region, and 0.128 ± 0.036 nm including all heavy atoms of the helical region. The average sum of all violations for these structures is 0.76 nm, whereas the average distance restraint violation is 0.0067 nm. Fig. 5*A* shows a superposition of the polypeptide backbone for the first 12 best structures of LAsCT: a unique backbone fold is obtained for residues 9–22, whereas lack of convergence is instead observed in the C terminus of the hormone and, to a lesser degree, in the N-terminal region. This reflects the absence of a sufficient number of NOEs, mainly due to the inherent flexibility of the molecule (14). In fact, the distribution of the observed NOEs along the LAsCT sequence indicates that the average number of constraints per residue is 5 for the Cys[1]–Val[8] region, 11 for the Leu[9]–Tyr[22] region, and 4 for the Leu[23]–Pro[32] region.

The distribution of the ϕ and ψ angles (data not shown) of the 12 lowest energy structures reflects the extent to which the conformation has been defined by NOE restraints. It shows a reduced dihedral dispersion in the α-helical region, whereas the Cys[1]–Val[8] and the Leu[23]–Pro[32] regions do not converge to a unique structure. For the C-terminal region, the progressive angular spreading and the NOE pattern justify the lack of convergence.

Structural information on the aggregate was obtained by using NOESY data. All NOEs were interpreted in a very conservative manner, and only those that were well resolved and clearly inconsistent with the global fold of the monomer were assigned as intermolecular contacts. In particular, we observed contacts between Leu[12] γCH and the Leu[19] δCH_3 (Fig. 5*B*), Thr[27] αCH and Leu[9] βCH_2 (Fig. 5*C*), and Thr[27] αCH and Leu[9] δCH_3. The Ser[13] βCH_2–Glu[15] γCH_2 NOE was also considered as an intermolecular contact: being the residues located on the opposite sides of the helix (Fig. 4*B*), the NOE contact gave rise to an unavoidable violation in the calculations of the monomer structure. The intermolecular NOEs were sufficiently well distributed to establish the antiparallel nature of the dimer. A starting structure was created by manually positioning two monomers with helices in an antiparallel arrangement, visually optimizing the orientation based on the above intermolecular NOEs. The starting structure was subjected to a series of simulated annealing runs. After analysis of energy and violations, the best 20 structures were energy-minimized, solvated in a periodic box of 5120 water molecules, and subjected to a 500-ps run of MD with all intra- and interchain restraint, followed by 1 ns of MD with interchain restraints only. The average r.m.s. deviation between the 20 best structure pairs is 0.081 ± 0.018 nm for the backbone atoms in the 9–22 region
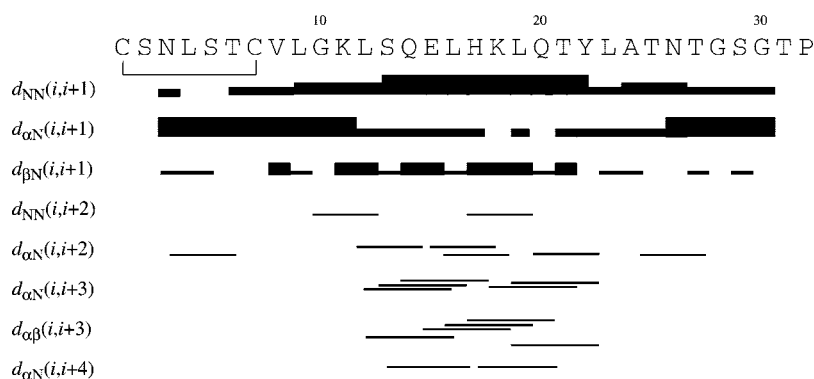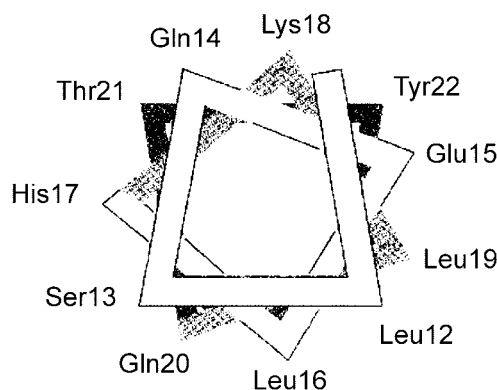
A

B

FIG. 4. **Sequential and medium range NOESY cross-peaks of LAsCT and wheel projection of the found helix.** *A*, sequential and secondary structural interresidues NOEs observed for LAsCT in ^1H_2O, ^2H_2O (90/10 v/v), 0.59 mM, 293 K, pH 7.4. NOE intensities are indicated by the *height* of the *bars*. *B*, helical wheel representation of the Leu[12]–Tyr[22] region of LAsCT.

and 0.136 ± 0.042 nm, including all heavy atoms of the helix. The average sum of all violations for these structures is 0.85 nm, whereas the average distance restraint violation is 0.0076 nm.

Fig. 5*D* reports the ribbon representation of the backbone atoms of the LAsCT dimeric region. It represents the average MD structure calculated on the last 250 ps of the simulation in water and exhibits an almost perfectly antiparallel orientation between the helices. The side chains of Leu[12] and Leu[19] from one monomer form hydrophobic layers with Leu[19] and Leu[12], respectively, of the other molecule. They are slightly offset because of the Leu[9]–Thr[27] interchain contact. These structural data confirm that the stability of the dimer depends upon hydrophobic interactions of Leu residues.

DISCUSSION

Amyloid fibrils formed by a diverse and structurally unrelated group of proteins share similar biophysical and structural properties, suggesting that self-assembly requires a specific pattern of molecular interaction. In fact, very short peptide fragments, hexa- and pentapeptides from islet amyloid polypeptide (3), amyloid β-peptide (4), tau protein (32), and hCT (5, 33), induce aggregation through hydrophobic and polar interactions and are crucial for fibril formation of the full-length peptides. Furthermore, model peptides not derived from

known fibril-forming proteins, but bearing hydrophobic residues and complementary charges, can form amyloid fibrils (6). Comparing the hydrophobicity with the amyloidogenic potential of various short peptides, the only apparent indication for potential amyloid fibril formation seems to be the presence of aromatic amino acids (5, 6), suggesting a role for aromatic residues in amyloid formation (6, 34, 35). In this context, calcitonin serves as an excellent model system to study the molecular recognition and self-assembly processes that lead to amyloid formation. In fact, hCT, which forms fibrils at pH 7.4, contains aromatic residues at sites 12, 16, 19, and 22, whereas sCT and LAsCT, which do not, both contain leucines at sites 12, 16, and 19.

We have demonstrated here that sCT and LAsCT form a dimer at pH 3.3 and 7.4 in aqueous solution. The structure was investigated by NMR spectroscopy and calculations, and we found that it corresponds to an antiparallel helical dimer stabilized mainly by hydrophobic interactions brought about by Leu[12] and Leu[19] (Fig. 5*D*), which are located 0.63 nm apart on both sides. It has been reported that in α-bundle proteins, leucine has the highest propensity in helix interfaces located at a distance >0.6 nm, and that Leu-Leu contacts dominate the pairwise interactions (36). The bundle motif is exemplified by the heptad repeat (**abcdefg**)$_n$ containing hydrophobic residues
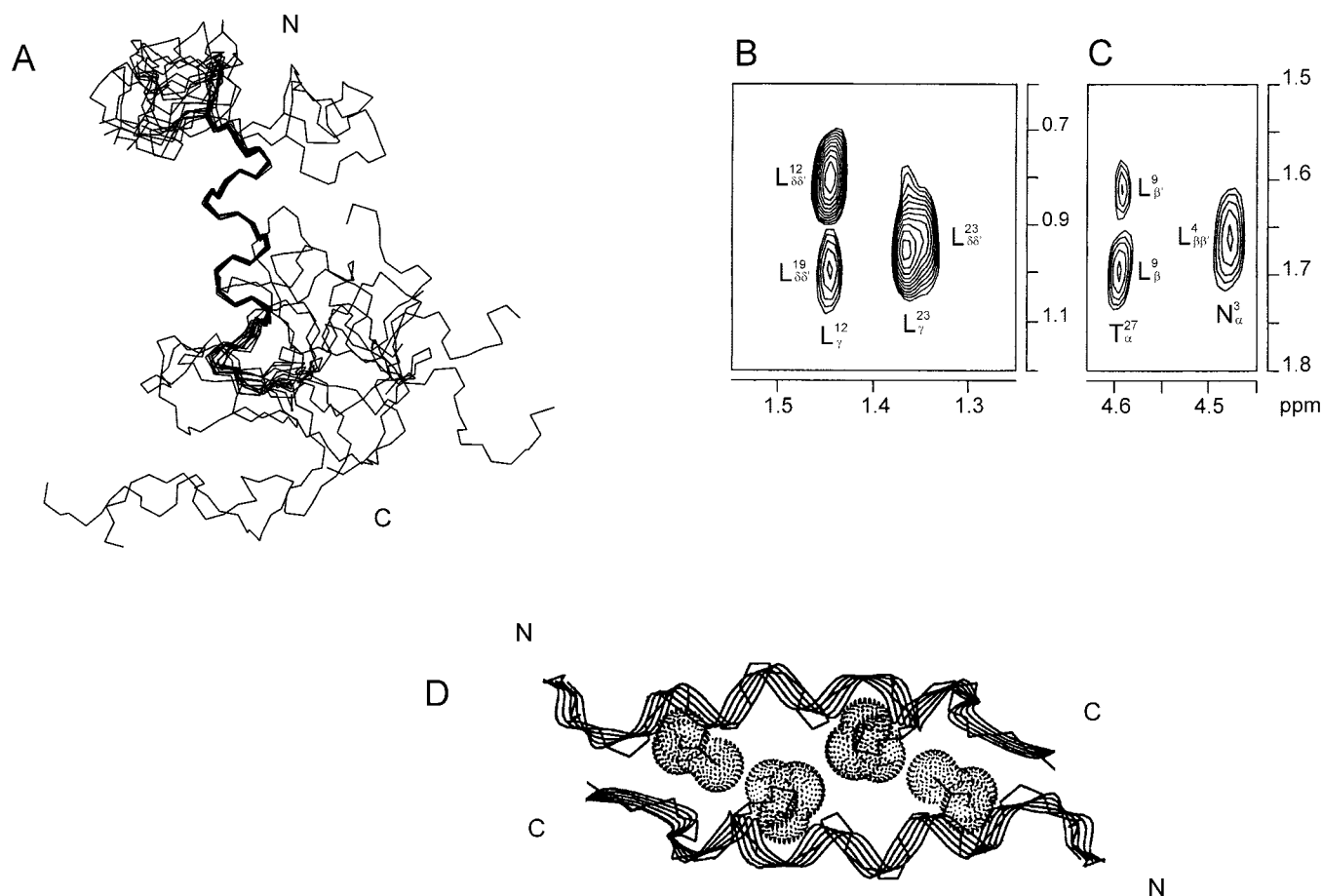
FIG. 5. **Calculated structures of LAsCT.** *A*, view of the Cα atoms of the 12 lowest energy structures of LAsCT. Structures were superimposed for pairwise minimum r.m.s. deviation of the Cα atoms of residues 9–22. The N and C termini are labeled. *B* and *C*, critical NOE contacts used to define the antiparallel nature of the LAsCT dimer. The aliphatic region of a 200-ms NOESY spectrum recorded at 293 K in water at pH 7.4 and a peptide concentration of 0.59 mM is shown. *D*, ribbon representation of the backbone atoms of the LAsCT dimer. It represents the average MD structure calculated on the last 250 ps of the simulation in water and was obtained with a best fit on residues 9–22.

at positions **a** and **d** and polar residues generally elsewhere. Analysis of left-handed coiled-coils shows that the predominant residue in the **a** and **d** positions of this motif is Leu (33%) (37), which also dominates the packing in helix-helix interactions (range >0.6 nm) in soluble proteins (36). Positions **b**, **c**, **e**, **f**, and **g** all bear hydrophilic residues and form the solvent-exposed part of the coil. Analysis of the primary structure indicates that sCT and LAsCT do have leucine zipper heptad repeats, whereas hCT does not (Scheme 2). In particular, Leu has a high relative occurrence in positions **a** and **d**, whereas Tyr and Phe have, respectively, a moderate and low occurrence (38). Furthermore, the **b**, **c**, **e**, **f**, and **g** positions correctly contain polar residues. The probability that the sequences in Scheme 2 can adopt a coiled-coil conformation was analyzed with COILS (39) (www.ch.embnet.org/software/coils/COILS-_doc.html). Although a predicted coil sequence should be regarded with some caution, the results reflect the coiled-coil-forming potential of a sequence. For sCT, we obtained an 85% probability in the region Leu[9]–Thr[21], whereas for LAsCT we obtained 93% probability in the region Leu[9]–Ala[24].

Nonetheless, no superhelical parameters (40) could be obtained for the LAsCT dimeric structure. We believe that this is due to the flexibility of the helix and to the shortness of the helical region (11 residues). Alternatively, the LAsCT structure could belong to the subgroup of antiparallel helical bundles that forms a true intermediate between coiled-coil and globular proteins (for example, the spectrin repeat (41)).

Except for Leu[9], hCT does not show the characteristic heptad

		a	b	c	d	e	f	g	a	b	c	d	e	f	g	a	b	c	d	e	f	g
Heptad		L	X	X	L	X	X	X	L	X	X	L	X	X	X	L	X	X	L	X	X	X
hCT		L	G	T	Y	T	Q	D	**F**	N	K	**F**	H	T	**F**	P							
sCT		L	G	K	L	S	Q	E	L	H	K	L	Q	T	Y	P							
LAsCT		L	G	K	L	S	Q	E	L	H	K	L	Q	T	Y	L	A	T				
		9			12				16			19				23						

SCHEME 2. **Comparison of the putative coiling regions of hCT, sCT, and LAsCT.**

repeat at the interior **a** and **d** positions occupied by aromatic residues (Scheme 2) whose relative occurrence in coils is low (38). In fact, prediction with COILS indicated that no region of hCT has the potential of forming a coiled-coil.

How are our results related to the CT fibrillation issue? hCT fibrillation kinetics are explained by a double nucleation model (8, 42): the early fibrillation phases involve aggregation of helical monomers to form a helix bundle that finally evolves into fibrils. Analysis of the fibrillation time *versus* the protein concentration indicates that four weakly interacting hCT molecules form the critical nucleus (43, 44). NMR studies (12) seem to suggest that hCT adopts an α-helical conformation in the initial fibrillation state and that the hydrophobic side of the helix (Met[8], Leu[9], Tyr[12], Asp[15], and Phe[16,19,22]) participates in the initial association step. Therefore, the initial cluster might be a helical bundle where the hydrophobic sides of the amphiphilic helices interact with each other. A possible formation of an α-helical structure during hCT fibrillation has also been inferred from CD results (8).

If the presence of a helix is required for fibrillation, why do the "helical" sCT and LAsCT not fibrillate, whereas the "non-helical" hCT does? We have observed that sCT and LAsCT are able to dimerize via the hydrophobic face of an amphipathic helix and that Leu-Leu interactions stabilize the aggregate and prevent fibril maturation. The central region of hCT does not assume a helical structure but forms instead a sequence of turns whose distance constraints are similar to those in helical peptide segments (30). NMR-based calculations (14) and solid-state NMR experiments (45) have confirmed the high mobility of the central region of hCT (Thr[13]–Phe[19]). Therefore, aggregation of hCT does not rely upon a specific secondary structure but on characteristic local, chemical properties. This is in line with the finding that short hCT peptides based upon the 15–19 region are able to form fibrils if Phe[16] and Phe[19] are preserved (5).

The sequence of turns in the central region of the monomer significantly limits the number of possible chain conformations and could thus provide an effective structural framework for the interaction of critical core residues. Collision of short helical-like stretches has been suggested as a mechanism for the folding pathways of GCN4p1 (46, 47). As a local factor, Gazit (35) has suggested that aromatic residues can provide two key elements for the formation of such structures: (i) an energetic contribution stemming from the π-stacking itself; and (ii) specific directionality and orientation provided by the specific pattern of stacking. As confirmation, an investigation of the early steps of fibril formation by islet amyloid polypeptide detected the stacking of aromatic rings just before the appearance of insoluble fibrils (48) and an alanine scan of the "basic amyloidogenic unit" of islet amyloid polypeptide demonstrated clearly the significant role of the phenylalanine residue (3). We suggest that, for an essentially unstructured polypeptide chain like hCT, orientation could be driven by the significant interaction between a hydrogen bond donor and the center of a benzene ring, which acts as a hydrogen bond acceptor (49). This interaction, which is about half as strong as a normal hydrogen bond, contributes $\sim$13 kJ mol^{-1} to the stability (49). Accordingly, intermolecular hydrogen bonds have been reported to play an important role in the association of the hCT molecules (12).

The dimeric structure found could serve a different purpose in sCT. At acidic and neutral pH, we observed a stable α-helix in the 12–19 regions, which dimerizes via hydrophobic interactions between leucine, as indicated by addition of guanidine HCl to CT solutions. This hydrophobic interaction in the prefibrillar state is sufficiently strong to prevent evolution toward fibril maturation. Our results indicate that leucines, but not aromatic residues, in the central segment of sCT favor a stable prefibrillar helical dimer that prevents amyloid formation. Therefore, we suggest that hCT fibril formation can be modulated by stabilizing the prefibrillar helical dimer in the transport fluid with insertion of leucine residues at sites 12, 16, and 19, in perfect agreement with the 20-fold increase of hCT hypocalcaemic potency obtained by replacing aromatic residues by leucine residues (15). On the other hand, if hCT fibrillation is avoided, an enhanced potency can be achieved (50), thus ruling out the need to use immunogenic fish calcitonins.

Finally, our finding strongly supports the recent hypothesis (17) that stabilization of α-helix/β-strand-discordant stretches (an α-helix in a polypeptide segment that should form a β-strand according to secondary structure predictions) into α-helix avoids amyloid fibril formation. In conclusion, we believe that altering the intermolecular recognition motifs in hCT may serve as a starting point for the design of inhibitors that avoid the amyloid formation process.

REFERENCES

1. Rochet, J. C., and Lansbury, P. T., Jr. (2000) *Curr. Opin. Struct. Biol.* **10,** 60–68
2. Taddei, N., Capanni, C., Chiti, F., Stefani, M., Dobson, C. M., and Ramponi, G. (2001) *J. Biol. Chem.* **276,** 37149–37154
3. Azriel, R., and Gazit, E. (2001) *J. Biol. Chem.* **276,** 34156–34161
4. Tjernberg, L. O., Callaway, D. J. E., Tjernberg, A., Hahne, S., Lilliehöök, C., Terenius, L., Thyberg, J., and Nordstedt, C. (1999) *J. Biol. Chem.* **274,** 12619–12625
5. Reches, M., Porat, Y., and Gazit, E. (2002) *J. Biol. Chem.* **277,** 35475–35480
6. Tjernberg, L., Hosia, W., Bark, N., Thyberg, J., and Johansson, J. (2002) *J. Biol. Chem.* **277,** 43243–43246
7. Benvegna, S., Trimarchi, F., and Facchiano, A. (1994) *J. Endocrinol. Invest.* **17,** 119–122
8. Arvinte, T., Cudd, A., and Drake, A. F. (1993) *J. Biol. Chem.* **268,** 6415–6422
9. Zaidi, M., Inzerillo, A. M., Moonga, B. S., Bevis, P. J., and Huang, C. L. (2002) *Bone (NY)* **30,** 655–663
10. Levy, F., Muff, R., Dotti-Sigrist, S., Dambacher, M. A., and Fisher, J. A. (1988) *J. Clin. Endocrinol. Metab.* **67,** 541–548
11. Kamihira, M., Naito, A., Tuzi, S., Nosaka, Y. A., and Saitô, H. (2000) *Protein Sci.* **9,** 867–877
12. Kanaori, K., and Nosaka, A. Y. (1995) *Biochemistry* **34,** 12138–12143
13. Siligardi, G., Samorì, B., Melandri, S., Visconti, M., and Drake, A. F. (1994) *Eur. J. Biochem.* **221,** 1117–1125
14. Amodeo, P., Motta, A., Strazzullo, G., and Castiglione Morelli, M. A. (1999) *J. Biomol. NMR* **13,** 161–174
15. Maier, R., Kamber, B., Riniker, B., and Rittel, W. (1976) *Clin. Endocrinol.* **5,** (suppl.) 327S–332S
16. Kallberg, Y., Gustafsson, M., Persson, B., Thyberg, J., and Johansson, J. (2001) *J. Biol. Chem.* **276,** 12945–12950
17. Epand, R. M., Epand, R. F., Orlowski, R. C., Schleuter, R. J., Boni, L. T., and Hui, S. W. (1983) *Biochemistry* **22,** 5074–5084
18. Andrade, M. A., Chacón, P., and Morán, F. (1993) *Protein Eng.* **6,** 383–390
19. Merelo, J. J., Andrade, M. A., Prieto, A., and Morán, F. (1994) *Neurocomputing* **6,** 443–454
20. Griesinger, C., Otting, G., Wüthrich, K., and Ernst, R. R. (1988) *J. Am. Chem. Soc.* **110,** 7870–7872
21. Jeener, J., Meier, B. H., Bachmann, P., and Ernst, R. R. (1979) *J. Chem. Phys.* **71,** 4546–4553
22. Hwang, T.-L., and Shaka, A. J. (1995) *J. Magn. Reson.* **112,** 275–279
23. Koning, T. M. G., Boelens, R., and Kaptein, R. (1990) *J. Magn. Reson.* **90,** 111–123
24. Weiner, S. J., Kollman, P. A., Case, D. A., Singh, U. C., Ghio, C., Alagona, G., Profeta, S., and Weiner, P. (1984) *J. Am. Chem. Soc.* **106,** 765–784
25. Ryckaert, J. P., Ciccotti, G., and Berendsen, H. J. C. (1977) *J. Comp. Phys.* **23,** 327–341
26. van Gunsteren, W. F., and Berendsen, H. J. C. (1977) *Mol. Physiol.* **34,** 1311–1327
27. Koradi, R., Billeter, M., and Wüthrich, K. (1996) *J. Mol. Graph.* **14,** 51–55
28. Cunningham, B. C., Mulkerrin, M. G., and Wells, J. A. (1991) *Science* **253,** 545–548
29. Arvinte, T., and Drake, A. F. (1993) *J. Biol. Chem.* **268,** 6408–6414
30. Wüthrich, K. (1986) *NMR of Proteins and Nucleic Acids*, pp. 162–170, John Wiley & Sons, Inc., New York
31. Otting, G., Qian, Y., Müller, M., Affolter, M., Gehring, W., and Wüthrich, K. (1988) *EMBO J.* **7,** 4305–4309
32. von Bergen, M., Friedhoff, P., Biernat, J., Heberle, J., Mandelkow, E.-M., and Mandelkow, E. (2000) *Proc. Natl. Acad. Sci. U. S. A.* **97,** 5129–5134
33. Kazantzis, A., Waldner, M., Taylor, J. W., and Kapurniotu, A. (2002) *Eur. J. Biochem.* **269,** 780–791
34. Gazit, E. (2002) *Curr. Med. Chem.* **9,** 1725–1735
35. Gazit, E. (2002) *FASEB J.* **16,** 77–83
36. Eilers, M., Patel, A. B., Liu, W., and Smith, S. O. (2002) *Biophys. J.* **82,** 2720–2736
37. Cohen, C., and Parry, D. A. (1990) *Proteins* **7,** 1–15
38. Langosch, D., and Heringa, J. (1998) *Proteins* **31,** 150–159
39. Lupas, A. (1996) *Methods Enzymol.* **266,** 513–525
40. Crick, F. H. C. (1953) *Acta Crystallogr.* **6,** 689–697
41. Yan, Y., Winograd, E., Viel, A., Cronin, T., Harrison, S. C., and Branton, D. (1993) *Science* **262,** 2027–2030
42. Hofrichter, J., Ross, P. D., and Eaton, W. A. (1974) *Proc. Natl. Acad. Sci. U. S. A.* **71,** 4864–4868
43. Bauer, H. H., Aebi, U., Häner, M., Hermann, R., Müller, M., Arvinte, T., and Merkle, H. P. (1995) *J. Struct. Biol.* **115,** 1–15
44. Arvinte, T. (1996) *Ciba Foundation Symposium*, Number 199, pp. 90–97, John Wiley & Sons, Inc., Chichester, UK
45. Kamihira, M., Yuki Oshiro, Y., Tuzi, S., Nosaka, A. Y., Saitô, H., and Naito, A. (2003) *J. Biol. Chem.* **278,** 2859–2865
46. Kammerer, R. A., Schulthess, T., Landwehr, R., Lustig, A., Engel, J., Aebi, U., and Steinmetz, M. O. (1998) *Proc. Natl. Acad. Sci. U. S. A.* **95,** 13419–13424
47. Vieth, M., Kolinski, A., Brooks, C. L., III, and Skolnick, J. (1994) *J. Mol. Biol.* **237,** 361–367
48. Kayed, R., Bernhagen, J., Greenfield, N., Sweimeh, K., Brummer, H., Voelter, W., and Kapurniotu, A. (1999) *J. Mol. Biol.* **287,** 781–796
49. Levitt, M., and Perutz, M. F. (1988) *J. Mol. Biol.* **201,** 751–754
50. Cudd, A., Arvinte, T., Das, R. E., Chinni, C., and MacIntyre, I. (1995) *J. Pharm. Sci.* **84,** 717–719

Modulating Calcitonin Fibrillogenesis: AN ANTIPARALLEL α-HELICAL DIMER INHIBITS FIBRILLATION OF SALMON CALCITONIN

Giuseppina Andreotti and Andrea Motta

Access the most updated version of this article at doi: 10.1074/jbc.M310882200

Alerts:
- When this article is cited
- When a correction for this article is posted

Click here to choose from all of JBC's e-mail alerts